Journal of Catalysis **205,** 299–308 (2002)
doi:10.1006/jcat.2001.3445, available online at http://www.idealibrary.com on IDEAL®

Characterization and Catalytic Properties of MAPO-36 and MAPO-5: Effect of Magnesium Content

M. da S. Machado,* J. Pérez-Pariente,†,[1] E. Sastre,† D. Cardoso,* M. V. Giotto,*,[2] J. L. García-Fierro,† and V. Fornés‡

*Chemical Engineering Department, Federal University of São Carlos, P.O. 676, 13565-905 São Carlos, SP, Brazil; †Instituto de Catálisis y Petroleoquímica, CSIC, Campus de Cantoblanco, 28049 Madrid, Spain; and ‡Instituto de Tecnología Química, UPV-CSIC, Avenida de los Naranjos s/n, 46022 Valencia, Spain

Received June 6, 2001; revised October 5, 2001; accepted October 10, 2001; published online January 9, 2002

Samples of MAPO-36 (ATS structure) and MAPO-5 (AFI structure) prepared with different magnesium contents and high crystallinity were characterized by several physical chemical techniques and catalytically evaluated using the isomerization of *m*-xylene as a reaction model. Chemical analysis of the solids indicated a greater incorporation of Mg into MAPO-5 than into MAPO-36 for the same Mg content in the gel. X-ray photoelectron spectroscopy results indicated that in both MAPOs the concentration of Mg at the surface is larger than that in the bulk in the as-synthesized samples, and that during the calcination process a depletion of the surface Mg has taken place. The calcination process of these samples caused Mg extraction from the framework of both materials. Infrared spectroscopy investigations of adsorbed pyridine showed that the acid strength of MAPO-36 is higher than that of MAPO-5, and that a high fraction of the acid sites disappears on calcining the samples in air. Temperature-programmed desorption of ammonia indicated the presence of two kinds of acid sites, the major part being strong acid sites which increase with Mg content. The catalytic activity of MAPO-36 decreases with the Mg content, which is attributed to a crystal size effect. The activity is much higher than that of MAPO-5 when the concentration of Mg in the crystals is small, but the difference decreases as the solids become richer in Mg.

Key Words: **MAPO-36; MAPO-5; synthesis; XPS; IR; NH_3–TPD; solid-state NMR; *m*–xylene isomerization.**

INTRODUCTION

MAPO-36 (ATS structure) is an aluminophosphate derivative having large micropores (6.5×7.4 Å) and unidirectional channels, in which part of the aluminum is substituted by magnesium atoms (1). This material is of special interest in catalysis, as it presents a catalytic activity much higher than those of other MAPOs, such as MAPO-5 and MAPO-11, in reactions such as *n*-butane cracking (2), *n*-hexane or iso-octane (3), and toluene disproportion (3, 4).

Notwithstanding the fact that the aforementioned investigations indicate that in general the catalytic activity of MAPO-36 is superior to that of MAPO-5, it would be interesting to compare the variation in activity of both materials as a function of the framework magnesium content. In the same way as in the case of zeolites the activity is influenced by the aluminum content of the framework; likely the activity and the stability of MAPO-type materials will depend on the concentration of magnesium in the framework.

In this work results are presented about the physical and chemical characterization of MAPO-36 and of MAPO-5 obtained with different Mg contents as well as their catalytic evaluation in the isomerization of *m*-xylene.

EXPERIMENTAL

Preparation of MAPOs

For both MAPOs the composition of the reaction medium was changed in order to obtain materials with different Mg contents in the solid. MAPO-36 was hydrothermally synthesized by a previously reported procedure (5) from reaction mixtures with the following molar composition:

$$2y\mathrm{MgO} : (1-y)\mathrm{Al_2O_3} : \mathrm{P_2O_5} : 4y\mathrm{HOAc} : 40\mathrm{H_2O} : r\mathrm{Pr_3N}. \quad [1]$$

The different gel compositions used in this work are detailed in Table 1. Synthesis of MAPO-36 was performed employing two distinct aluminum sources: pseudoboehmite (Pural SB Condea, Al_2O_3 74.6 wt%) and aluminum isopropoxide (Aldrich, 98 wt%). When pseudoboehmite was used (samples denoted as P), the Mg concentration was varied in the range $y = 0.026$–0.183. When aluminum isopropoxide was used (samples denoted

[1] To whom correspondence should be addressed. Fax. 34 91 585 47 60. E-mail: jperez@icp.csic.es.

[2] Present address: Carlson School of Chemistry, Clark University, Worcester, Massachusetts 01610.

0021-9517/02 $35.00

TABLE 1

Properties of MAPO-36 (Samples P and I) and MAPO-5 (Samples M)

	$x = Mg/(Mg + Al + P)$					Crystallinity (%)					
			Framework[b]			Uncalcined		Calcined		Pore volume ($cm^3\ g^{-1}$)	
Sample	Gel	Solid[a]	Uncalcined	Calcined	Template (r)	ATS	AFI	ATS	AFI	Micro	Macro + meso
P26	0.013	0.012	nd	0.012	2.4	65	*t*	50	*t*	0.098	0.220
P03	0.033	0.025	0.028	0.021	1.8	77	*t*	74	*t*	0.136	0.149
P04	0.043	0.030	—	—	1.8	81	*t*	76	*t*	0.123	0.159
P05	0.053	0.040	—	—	1.8	82	0	77	0	0.135	0.105
P07	0.073	0.051	0.051	0.030	1.8	87	0	83	0	0.143	0.094
P09	0.093	0.057	—		1.8	85	0	80	0	0.135	0.088
I03	0.033	0.026	—		1.8	70	10	60	15	0.122	0.146
I05	0.043	0.043	0.041	0.024	1.8	88	10	74	16	0.138	0.116
I08	0.053	0.052			1.8	90	*t*	70	*t*	—	—
M0	0.005	0.014	nd	0.008	1.5	0	100	—	95	0.050	0.021
M1	0.027	0.044	—	—	1.35	0	95	—	83	0.115	0.022
M2	0.054	0.072	0.051	0.026	1.5	0	95	—	80	0.120	0.016
M3	0.077	0.077	—	—	1.25	0	95	—	70	0.126	0.008
M4	0.100	0.086	0.048	0.018	1.0	0	95	—	68	0.119	0.001

[a] Determined by elemental analysis.
[b] Determined by ^{31}P MAS NMR.

as I), the concentration of Mg ranged from $y = 0.066$ to 0.106.

On the other hand MAPO-5 was synthesized according to a procedure reported by Concepción *et al.* (6), from reaction mixtures with the following composition,

$$y\mathrm{MgO} : 0.8\mathrm{Al_2O_3} : \mathrm{P_2O_5} : z\mathrm{H_2O} : r\mathrm{Et_3N}, \qquad [2]$$

using pseudoboehmite as an aluminum source (samples denoted as M). The Mg content was varied in the range $y = 0.02$–0.4 with $z = 47$ or 120. Pure $AlPO_4$ was prepared without adding Mg to the gel. The template (r) content in the reaction mixtures to obtain both MAPOs is listed in Table 1. Crystallization was carried out under static conditions and for MAPO-36 two heating steps were used: initially for 50 h at 373 K and then for 24 h at 423 K. Due to the greater difficulty in producing MAPO- 36 with low Mg content (P26, Table 1), this material was crystallized at 373 K for 120 h and at 423 K for 48 h (5). MAPO-5 was always crystallized at 463 K from 16 to 40 h. The solid product was recovered by centrifugation, washed with deionized water, and dried at 373 K overnight.

The organic template occluded within the MAPO channels was removed by calcining the samples, about 1 g of solid, at a heating rate of 2 K min^{-1} in N_2/air (60 ml min^{-1}). Calcination of MAPO-5 was carried out at 813 K, initially under a nitrogen flow for 4 h and then under air flow for 6 h more. For the complete elimination of the MAPO-36 template, calcination was first performed in nitrogen atmosphere for 2 h at 523 K and for an additional 4 h at 673 K. After this step the sample was calcined in air flow at 813 K for 24 h.

Characterization

The X-ray diffractograms (XRD) of the samples were obtained in a Philips PW 1710 diffractometer using Cu$K\alpha$ radiation. Crystallinity of the MAPO-36 materials was determined as described in Ref. 5. Crystallinity of the MAPO-5 samples was determined by dividing the area underneath the peaks at $2\theta = 19.8$, 21.1, and 22.4° by the area of the standard sample (M0).

Elemental analysis of aluminum, magnesium, and phosphorous was performed by plasma emission induced spectrophotometry. In order to check for the eventual loss of magnesium in the solid during calcination (7), both calcined and noncalcined samples were analyzed, but no substantial changes were observed.

Temperature-programmed desorption of ammonia (NH_3–TPD) experiments were performed in a Micromeritics Model 2900 using the following conditions: 100 mg of calcined sample was activated in an O_2 stream at 723 K for 3 h, and after cooling the NH_3 was adsorbed at 373 K. The temperature was then increased to 1100 K at a heating rate of 10 K min^{-1} under helium as carrier gas at a flow of 100 ml min^{-1}. The desorption process was monitored by means of a thermal conductivity detector (TCD) and a mass spectrometer (Balzers). In order to verify the presence of other desorption products besides ammonia, such as dehydroxylated water, a blank run was performed for each sample using the same desorption program but without previous adsorption of NH_3.

Infrared spectra of the MAPOs containing adsorbed pyridine were obtained in a Nicolet 710 FTIR spectrophotometer. Adsorption and desorption of pyridine were

performed using 10 mg cm^{-2} wafers of the pure sample. In order to eliminate water and eventually adsorbed organic material, the samples were pretreated at 673 K overnight in vacuum ($\sim 10^{-3}$ Pa). Adsorption of pyridine (5×10^{-2} Pa) was performed at room temperature. Once the physisorbed fraction was eliminated at room temperature, the spectrum was recorded at room temperature. The desorption step of chemisorbed pyridine was performed *in vacuum* for 1 h at 523, 623, and 673 K. The spectra were recorded at room temperature after cooling of the samples.

The adsorption and desorption isotherms of nitrogen were obtained at 77 K using a Micromeritics ASAP 2000. The samples were previously degassed overnight *in vacuum* at 623 K.

XPS analysis was carried out in a Fisons Escalab MkII 200R spectrometer, equipped with a semispherical electron analyzer and a Mg anode X-ray emission source (Mg$K \propto = 1253.6$ eV), supplied with 12 kV and 10 mA. The measurements were performed operating at a residual pressure of less than 6×10^{-7} Pa in the analysis chamber.

Calcined samples were dehydrated to perform all NMR experiments. The drying process was developed using an oven at 383 K for 14 h. The 7-mm NMR rotors with two rubber o-rings were filled with dehydrated samples and handled carefully. Solid-state ^{31}P and ^{27}Al MAS NMR spectra of dehydrated samples were acquired using a Varian Unity Plus 400-MHz spectrometer operating at 161.90 and 104.21 MHz, respectively, and chemical shifts were quoted from H_3PO_4 85 wt% and $Al(H_2O)_6^{3+}$. Recycle times were 60 and 2 s for ^{31}P and ^{27}Al, respectively, with 200 transients, 100 kHz of bandwidth, and a MAS of 8 kHz. Phosphorus spectra were obtained with high-power proton decoupling using a pulse length of 4.0 μs ($\pi/4$). ^1H–^{31}P CP MAS NMR spectra were performed using a ^1H pulse length of 4.5 μs ($\pi/2$) with a contact time of 5 ms, 200 transients, and recycle times of 10 s. Aluminum spectra were obtained with selective excitation using a short pulse of 1 μs ($\pi/20$).

Catalytic Activity

Isomerization of *m*-xylene took place in a fixed-bed reactor at atmospheric pressure, working with a temperature of 623 K and a molar ratio of N_2/*m*-xylene = 4. The contact time was varied accordingly to obtain conversions of approximately 5%. The reaction products were analyzed by gas chromatography in a GC Varian 3700. This was provided with a flame-ionizing detector and equipped with a column filled with DC-200 methylsilicone (16%) and Bentone 34 (3%) on Chromosorb W (80–100 mesh). In order to compare the activity of the catalysts in the absence of deactivation, the initial activity (V_0) of all products was calculated by extrapolating the conversion at time zero of reaction (8).

RESULTS AND DISCUSSION

Some properties of the MAPO-36 and MAPO-5 samples are listed in Table 1. Both materials present a drop in crystallinity after calcination. This drop is more pronounced for the MAPO-5 samples obtained with higher magnesium contents in the solid, i.e., $x > 0.072$, indicating that, as already reported by other authors (6, 9), the stability of the framework decreases as the magnesium content increases. For MAPO-36, the samples obtained with aluminum isopropoxide (I samples) are seen to be less stable to calcination than those obtained by using pseudoboehmite as an aluminum source (P samples). As aluminum isopropoxide is more reactive in producing MAPO-36, the crystals formed when this source was used possibly present more defects and are therefore less stable. Compared to the micropore volumes previously reported for the AFI and ATS materials (9, 10), the experimental values obtained by N_2 adsorption (Table 1) show, in general, a reasonable stability of the structure after calcination. On the other hand, the decrease in volume of mesopores as the Mg content increases is likely due to the increase in crystal size, as reported previously (5).

The bulk content of Mg in the solids for MAPO-36 and MAPO-5 as a function of the molar fraction of this element in the gel is presented in Fig. 1. The Mg content in the solid increases with the molar fraction of this element in the gel, and in the case of MAPO-36 a linear relationship is observed. It is also seen that, although the synthesis conditions of the two materials are not alike, for the same Mg content in the gel, there is a larger incorporation of Mg into MAPO-5 when compared to MAPO-36. This stronger affinity of the AFI structure to magnesium might be the reason why MAPO-5 crystallizes concurrently with MAPO-36 when the concentration of this element in the gel is very small (5). Unlike Prasad *et al.* (7), who observed a loss of as much as 40% of Mg present in the solid during calcination of MAPO-36, no variation has been observed for the

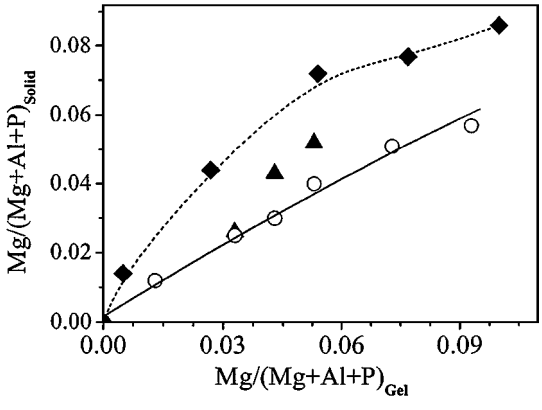

FIG. 1. Magnesium content in solid and in gel. MAPO-36 from pseudoboehmite (○), isopropoxide (▲), and MAPO-5 (◆).

TABLE 2

XPS Results for the Synthesized and Calcined Samples of MAPO-36 and MAPO-5

Sample[a]	x^b Bulk	x^b $Surface_{XPS}$	w^c XPS	Binding Energy (eV) Al_{2p}	P_{2p}	Mg_{2p}
P26	0.012	0.012	0.595	74.5	134.1	49.9
P05	0.040	0.080	0.575	74.4	134.1	50.1
P26C	0.012	0.050	0.575	74.4	134.1	49.8
P05C	0.040	0.025	0.617	74.4	134.1	49.7
M0	0.014	0.065	0.463	74.4	133.9	50.1
M1	0.044	0.072	0.448	74.3	133.9	49.8
M0C	0.014	0.054	0.450	74.4	133.9	50.1
M1C	0.044	0.056	0.429	74.4	133.9	50.0

[a] C, calcined.
[b] $x = Mg/(Mg + Al + P)$.
[c] $w = Al/(Mg + Al + P)$.

magnesium content in the solid after calcination of the samples presented in Fig. 1.

The surface composition of the elements present in the MAPO-36 and MAPO-5 samples determined by XPS measurements are listed in Table 2.

The results of the as-synthesized samples show that the fraction of magnesium at the surface is in general higher than that at the bulk. However, in the case of MAPO-5 there is proportionally a higher concentration of magnesium at the surface of the sample with lower Mg content in the solid. Consequently, the fraction of surface aluminum decreases with the increase in Mg content, indicating isomorphic substitution. However, in the case of MAPO-36 the fraction of Al is higher than 0.5, indicating the existence of extra-framework Al, possibly originated from unreacted pseudoboehmite (11). The concentration of Mg at the surface decreases after calcination, with the exception of sample P26. The binding energies of Al_{2p}, 74.4 ± 0.1 eV, and P_{2p}, 134 ± 0.1 eV, are characteristic of these elements in tetrahedral coordination in AlPOs structures (12). Finally, the binding energy of Mg_{2p} (49.9 ± 0.2 eV) is very close to that reported for tetrahedrally coordinated Mg in the $MgAlO_4$ spinel structure, which indicates a tetrahedral coordination of this element in the MAPO-36 and MAPO-5 structures, respectively (13, 14).

Nuclear Magnetic Resonance Spectroscopy

The ^{31}P MAS NMR spectra of some calcined and dehydrated samples of MAPO-36 and MAPO-5, whose properties are listed in Table 1, are shown in Fig. 2. The ^{31}P MAS NMR spectra of the MAPO-36 samples (Fig. 2a) exhibit a resonance at -27.7 ppm attributed to the P(4Al) and a shoulder at -21.3 ppm which can be attributed to P(3Al, 1Mg) sites in the ATS framework (7). On the other hand, in the case of MAPO-5 (Fig. 2b), similar spectra are observed with resonances at the chemical shifts -29.8 and -22.6 ppm, assigned to sites P(4Al) and P(3Al, 1Mg) in the AFI framework (11). Moreover, there is a small signal at 0 ppm for the two samples with high incorporation of Mg in the framework, M2 and M4, which can be attributed to nonzeolitic phosphate species, as reported previously (11).

Deconvolution of the ^{31}P MAS NMR spectra enables one to estimate the fraction of Mg, $x = Mg/(Mg + Al + P)$, incorporated in the ATS and AFI framework of the calcined samples, and the results are presented in Table 1. In this table are also listed the fractions of framework Mg present in the as-synthesized samples, the determination of which is presented elsewhere (11, 15). It can be observed that a maximum value of 5% of Mg can be incorporated into the as-synthesized MAPO-5 crystals. However, during the calcination process of both MAPOs part of the magnesium is removed from the crystalline framework, remaining in the samples as extra-framework species. Magnesium removal

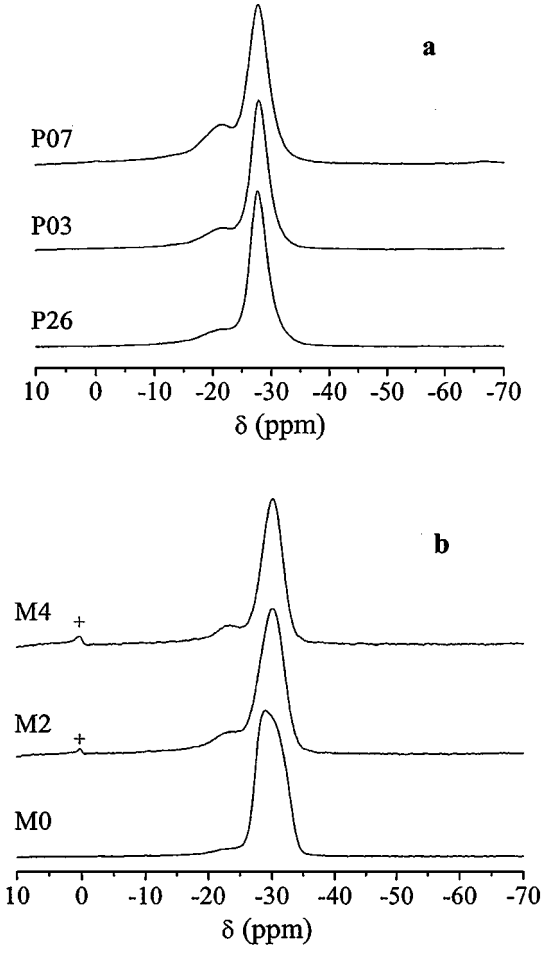

FIG. 2. ^{31}P MAS NMR spectra of calcined samples with different Mg_{solid} contents (indicated in parentheses). (a) MAPO-36, sample P26 (0.012); P03 (0.025); P07 (0.051). (b) MAPO-5, sample M0 (0.014); M2 (0.072); M4 (0.086). Contact time 5 ms.

from the framework was more pronounced for the samples with higher Mg contents, which indicates that the stability of the crystalline structure decreases as the Mg content is increased. This result was also confirmed by the drop in crystallinity of these samples (Table 1) determined by X-ray diffraction.

The presence of Mg in the crystalline framework of the calcined MAPOs, generating P(3Al, 1Mg) species, becomes more evident in the cross-polarized ^{1}H–^{31}P CPMAS NMR experiments (Fig. 3). Compared to Fig. 2, these spectra exhibit an increase in the intensity of the resonances at −21.9 and −23.3 ppm for MAPO-36 (Fig. 3a) and MAPO-5 (Fig. 3b), respectively. Prasad *et al.* (7) in ^{31}P MAS NMR studies of calcined MAPO-36 samples using cross polarization also observed a resonance at −21.6 ppm and attributed this to the substitution of magnesium for aluminum atoms, contrary to the former attribution of this signal to P atoms interacting with adsorbed molecules (16).

In Fig. 3b it can also be noticed that the MAPO-5 sample containing the lowest amount of Mg (sample M0) exhibits a signal centered at ca. −20 ppm, instead of at −23.3, accompanied by an additional peak of lower intensity at ca. −14 ppm. Indeed, the ^{1}H–^{31}P CP spectrum of the MAPO-36 sample with the lowest Mg content presents an asymmetric ^{31}P peak, with a broad ill-defined signal at ca. −15 ppm. These signals have also been detected in calcined AlPO-5 (11) and can be assigned to P–OH species.

Figure 3c shows the ^{31}P MAS NMR spectra as well the corresponding ^{1}H–^{31}P CPMAS of sample I05 (Table 1) of MAPO-36 obtained with aluminum isopropoxide. These spectra are very similar to those of sample P03 prepared with pseudoboehmite (Fig. 3a) which has a similar framework composition (Table 1), confirming the incorporation of magnesium in the ATS framework regardless of the aluminum source employed in the synthesis.

Figure 4 shows the ^{27}Al MAS NMR spectra of the calcined and dehydrated samples of MAPO-36 and MAPO-5. The spectra present an intense signal in the 38.5 and 37.6 ppm region for the MAPO-36 and MAPO-5 samples, respectively, typical of tetrahedrally coordinated aluminum (11). The absence of resonances at around −12 ppm reported by Montoya-Urbina *et al.* for SAPO-5 (17), related to framework octahedral aluminum species coordinated with two water molecules, indicates the efficiency of the dehydration procedure. In the case of the MAPO-36 spectra (Fig. 4a) a broad additional resonance at around 6.5 ppm is observed which may be attributed to a small fraction of unreacted pseudoboehmite in the MAPOs (11) and occurs typically in some AlPO derivatives (17). In the case of MAPO-5 the ^{27}Al MAS NMR spectra do not exhibit signals at around −6.5 ppm, probably due to the lower aluminum content used in the reaction mixture compared to that of MAPO-36 (Eqs. [1] and [2], respectively).

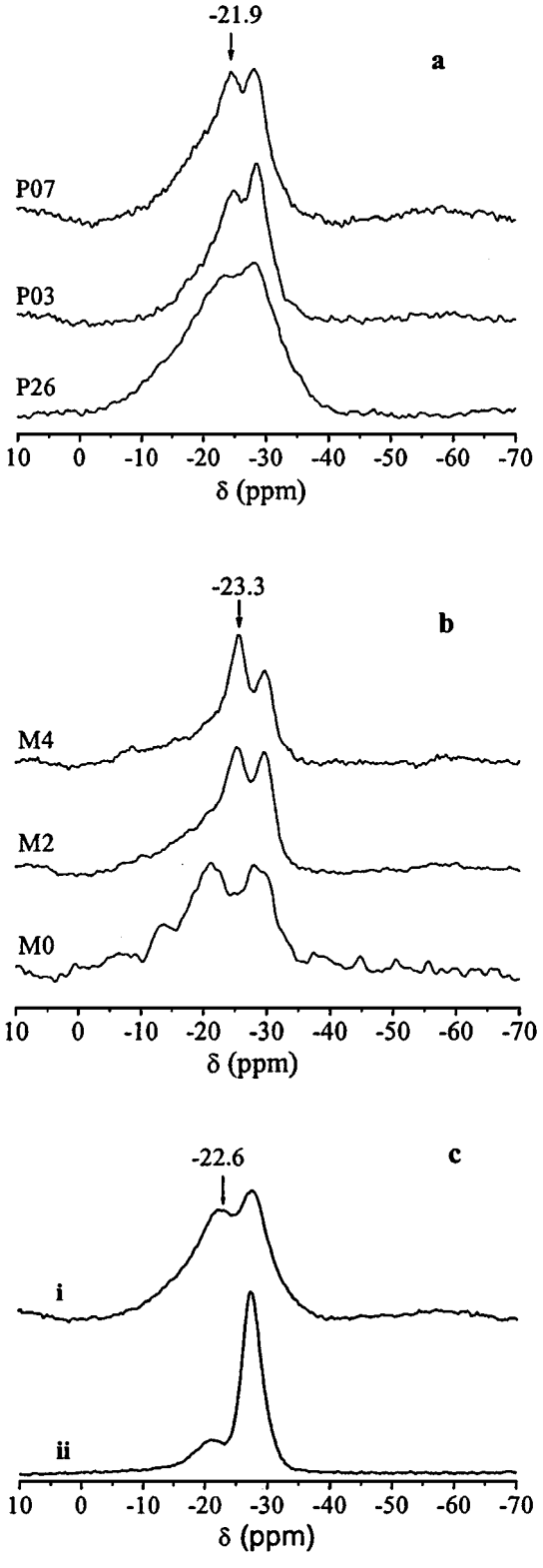

FIG. 3. ^{1}H–^{31}P CP MAS NMR (contact time 5 ms) spectra of calcined samples with different Mg_{solid} contents (indicated in parentheses). (a) MAPO-36, sample P26 (0.012); P03 (0.025); P07 (0.051). (b) MAPO-5, sample M0 (0.014); M2 (0.072); M4 (0.086). (c) MAPO 36, sample I05 (0.043): i, ^{1}H-^{31}P CP MAS NMR (contact time 5 ms). ii, ^{31} P MAS NMR spectra.

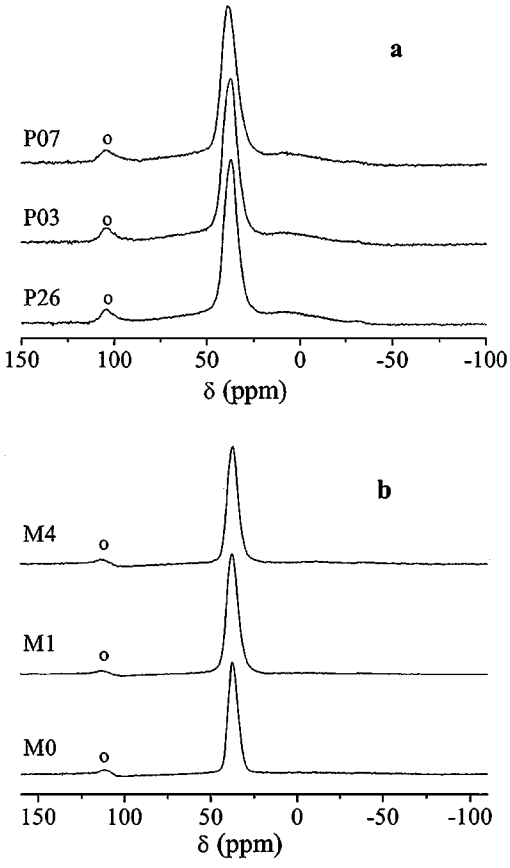

FIG. 4. ^{27}Al MAS NMR spectra of calcined samples with different Mg contents (indicated in parentheses). (a) MAPO-36, sample P26 (0.012); P03 (0.025); P07 (0.051). (b) MAPO-5, sample M0 (0.014); M2 (0.072); M4 (0.086). o denotes signal of the Si_3N_4 rotor.

Infrared Spectroscopy

Figure 5 shows the infrared spectra of the pyridine adsorbed on MAPO-36 with different amounts of framework Mg, calcined *in vacuum* in the IR cell. From this figure it can be concluded that the Brønsted acidity of MAPO-36 (band at 1545 cm^{-1}) is related to the amount of Mg in the structure, as expected. With the increase of desorption temperature the intensity of this band is reduced, but a relatively high fraction of pyridine still remains adsorbed at 673 K indicating that, as previously reported in the literature (4, 18–20), MAPO-36 contains strong acid sites. Exposure of the samples to the atmosphere after calcination produces a damage in the crystal structure partially removing framework Mg and, as a consequence, decreasing the number of Brønsted acid sites (Fig. 6). The presence of Lewis acid sites is confirmed by the appearance of two IR bands at 1448 and 1612 cm^{-1} corresponding to pyridine coordinated to Mg ions. Moreover, the bands of lower intensity appearing at 1454 and 1622 cm^{-1} are the equivalents for Al ions.

The equivalent spectra for MAPO-5 (Fig. 7) clearly show that, unlike MAPO-36, the band of protonated pyridine at 1545 cm^{-1} practically disappears at 673 K, indicating that this structure has weaker Brønsted acid sites than those of MAPO-36.

Temperature-Programmed Desorption of Ammonia

The NH_3–TPD curves of three calcined samples of MAPO-36 are shown in Fig. 8. There the presence of four desorption bands can be detected (A, B, C, and D) at temperatures around 540, 630, 840, and 1000 K. The first desorption maximum (A) coincides with that of ammonia

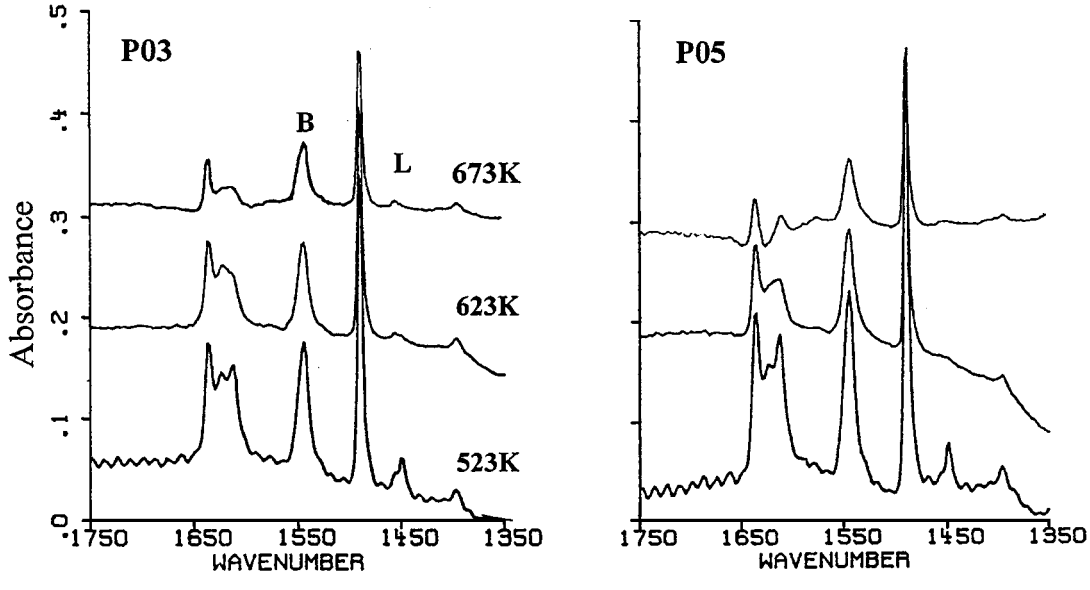

FIG. 5. IR spectra of MAPO-36 prepared with pseudoboehmite, calcined *in situ* and with adsorbed pyridine at 523, 623, and 673 K.

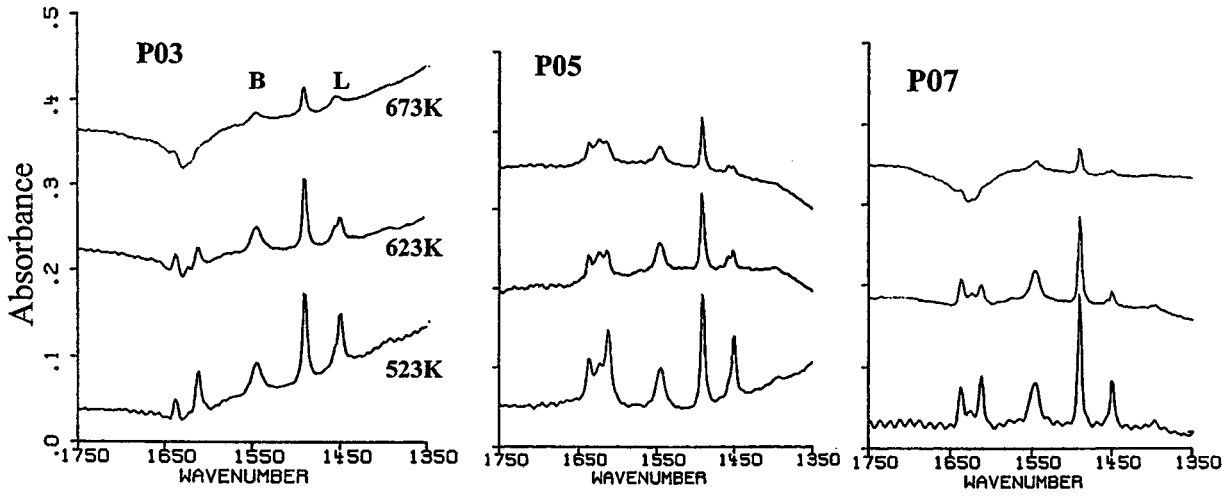

FIG. 6. IR spectra of MAPO-36 prepared with pseudoboehmite, exposed to the environment and with adsorbed pyridine at 523, 623, and 673 K.

desorption in AlPO-5 (19) and can be attributed to weak active sites associated to POH groups and Al and Mg located in structural defects. Band B, not present in AlPOs, can be tentatively assigned to desorption of ammonia on Brønsted acid sites originated by isomorphic substitution of Al^{3+} by Mg^{2+} in the MAPO structures. This band appears at lower temperatures (480 K) in MAPO-5 (6, 21), indicating that MAPO-36 possesses stronger acid sites in good agreement with the pyridine adsorption results (see previously). Bands C and D correspond to water formed by dehydroxylation of MAPO-36 in agreement with the results presented in Fig. 9. In this figure we compare the TPD–Mass spectra of NH_3 (Mass 15) and H_2O (Mass 18) with the TCD signal vs temperature for the P07 sample showing that the last two bands are due exclusively to water. These bands have not been observed previously (18–20), probably due to the fact that the TPD experiments were interrupted below 800 K.

The amounts of adsorbed ammonia from the MAPO- 36 samples are listed in Table 3. From these results it can be observed that the sample with the highest content of framework magnesium (P07) exhibits the largest amount of ammonia adsorbed on the strong acid sites. These results corroborate those previously discussed for IR spectra, in which an increase of the band at 1545 cm^{-1} was observed, as the magnesium content in the solid was higher. The total number of acid sites is also seen to increase as the magnesium content in the framework increases.

Catalytic Activity

The initial activity of *m*-xylene isomerization as a function of the magnesium content in the solid for MAPO-36 obtained with pseudoboehmite (P samples) and aluminum isopropoxide (I samples) is shown in Fig. 10. The reaction was performed with samples calcined *in situ* (curves *a* and *d*) as well as with samples calcined *ex situ*. The activity of

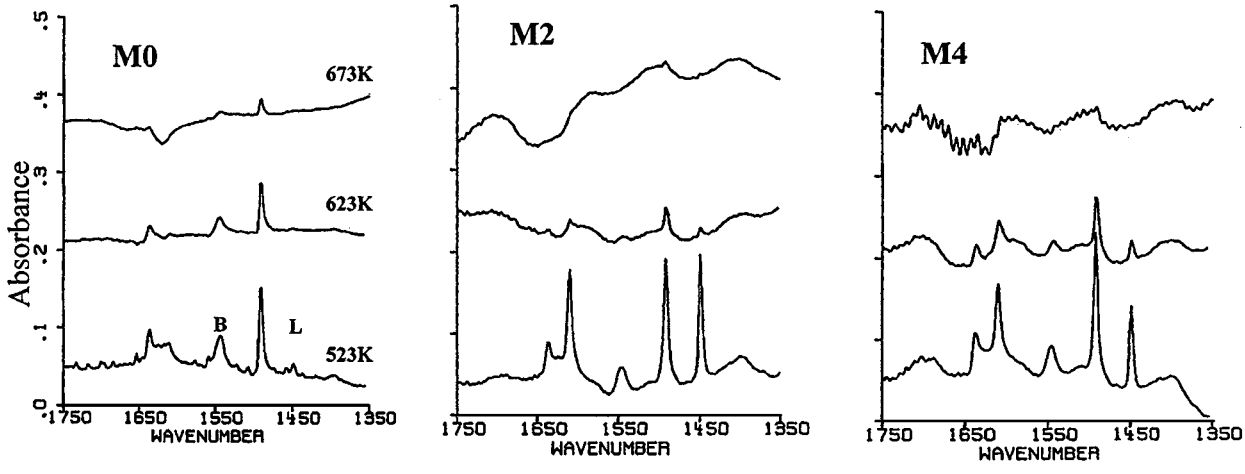

FIG. 7. IR spectra of MAPO-5 exposed to the environment and with adsorbed pyridine at 523, 623, and 673 K.

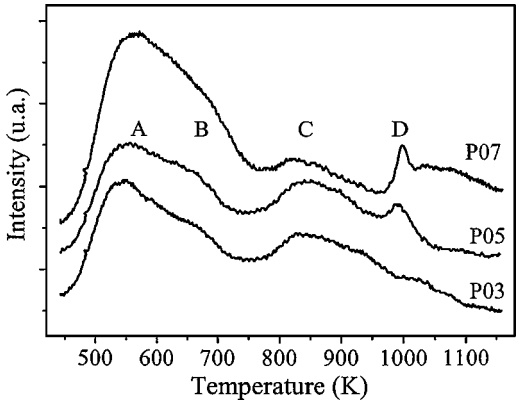

FIG. 8. TPD of ammonia for the MAPO-36 samples calcined *ex situ*.

the *ex situ* calcined samples was determined immediately (curve *b*) or after storing for 1 year (curve *c*). In the case of samples synthesized from aluminum isopropoxide, the activity in Fig. 10 is shown for a molar fraction of magnesium in the solid higher than 0.02. Using this aluminum source, it was not possible to obtain pure MAPO-36 with lower magnesium content (5).

From the Fig. 10 it can be seen that, for the four sets of samples, the initial activity presents a maximum, which appears at very low Mg content (x of the solid ≈ 0.012). In a first approach, the activity should increase with the acidity. Nevertheless, it has been discussed earlier that the Brønsted acidity increases with the magnesium content of the MAPO-36 crystals. Therefore, another factor should affect the catalytic activity of the sample. This effect could not be due to an eventual loss of crystallinity, which actually increases with the magnesium content, particularly in the range of 0.012–0.025. On the other hand, it can be observed in Table 1 that the pore volume corresponding to pores larger than micropores is very high for the MAPO-36 with the lowest magnesium content and decreases systematically as the crystals become richer in this metal. Therefore, an optimum accessibility to the acid sites would take place for

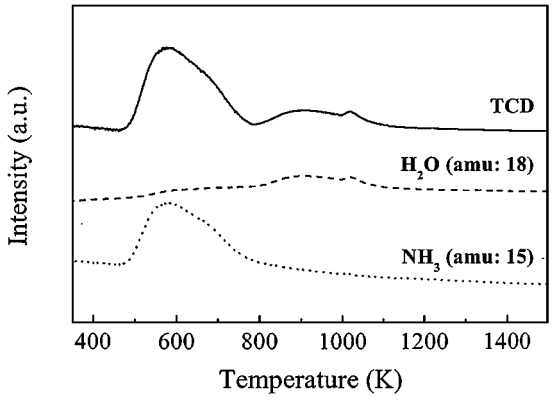

FIG. 9. TCD signal and TPD–MS of NH_3 (Mass 15) and H_2O (Mass 18) vs temperature for P07 sample.

TABLE 3

TPD of Ammonia of MAPO-36 Samples Calcined *ex Situ*

Sample	Mg/(Mg + Al + P)		Adsorbed NH_3 (10^5 mol g_{cat}^{-1})		
	Solid	Framework	Total acidity	Weak acidity[a]	Strong acidity[a]
P03	0.025	0.021	58	20	38
P05	0.040	—	59	20	39
P07	0.051	0.030	102	20	82

[a] Weak acidity = ammonia desorption in peak A. Strong acidity = peak B.

the sample with the lowest magnesium content. This effect would be particularly important for monodirectional crystalline microporous materials, such as MAPO-36. Indeed, the beneficial influence of the generation of mesopores by acid leaching in dealuminated mordenite for the hydroisomerization of *n*-hexane has been recently reported (22). As related to the mesoporosity, it has been reported in Ref. 5 that the MAPO-36 is formed by thin needle-shape crystals, which agglomerate into spherical aggregates, whose diameter increases with the Mg content from 20 to 100 μm. In summary, we believe that the *m*-xylene conversion is likely affected by diffusional constraints, the severity of which increases with the crystal size and hence with the Mg content.

The activity of MAPO-36 decreases when the samples are calcined *ex situ* (curve *b*). The reduction in activity is likely a consequence of the instability of Mg in the ATS framework, which is partially removed from the framework by hydrolysis during manipulation of the catalyst. These results are in agreement with the reduction in intensity of the Brønsted acid band at 1545 cm^{-1} and the increase of the Lewis band at 1448 cm^{-1} in the IR spectra discussed earlier (see Figs. 5 and 6). For the samples exposed to air for a long time the activity is considerably reduced (curve *c*), which indicates a greater loss of framework Mg with exposure time. The parallelism between the activity curves of the samples calcined *in situ* and those stored for long periods (curves *a* and *c*) suggests that the fraction of Mg removed from the framework is nearly constant.

Figure 10 shows also that the samples obtained employing aluminum isopropoxide and calcined *in situ* (curve *d*) are less active than those with the same magnesium content in the solid and calcined under the same conditions, but obtained with pseudoboehmite (curve *a*). The lower activity of the isopropoxide samples might also be due to crystal size effects, although in this case the aggregates are more irregular in size and shape (5).

In Fig. 11 the results of activity of MAPO-5 and MAPO-36 (samples P), both prepared from pseudoboehmite, are compared as a function of Mg in the solid. The result shows that up to intermediate Mg contents MAPO-36 is much more active than MAPO-5, which is consistent with the stronger acidity of MAPO-36. Similar results have been

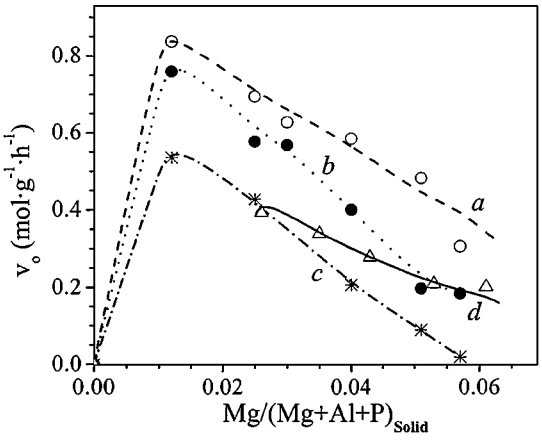

FIG. 10. Influence of magnesium content of MAPO-36 on *m*-xylene conversion activity. ○, P samples (pseudoboehmite) calcined *in situ*, curve *a*. ●, P samples calcined *ex situ,* curve *b*. (∗) These last samples after 1 year, curve *c*. △, Samples prepared from aluminum isopropoxide (I) calcined *in situ,* curve *d*.

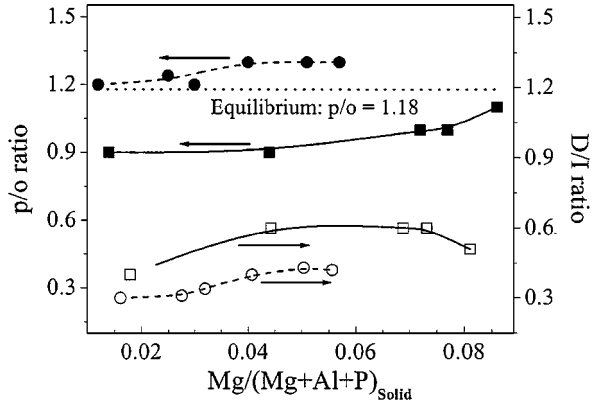

FIG. 12. Selectivity on the MAPOs. p/o-xylene ratio of ●, MAPO-36 and ■, MAPO-5. D/I ratio of ○, MAPO-36 and □, MAPO-5.

encountered by other authors in the cracking reactions of *n*-butane (2) and in the conversion reactions of linear alcohols (3). On the other hand, the activity of MAPO-36 decreases as the magnesium content in the solid increases, whereas that of MAPO-5 increases continuously and only decreases at high Mg content, in such a way that for a Mg fraction >0.07, the activity of both materials is similar. Contrary to what has been observed for MAPO-36 (Fig. 10), the activity of MAPO-5 did not vary significantly when calcination was performed *ex situ*.

Figure 12 presents the selectivity to para- and orthoxylene isomers as well as disproportion/isomerization (D/I) as a function of the magnesium content in the solid of samples calcined *in situ*. In the case of MAPO-5 the p/o ratio is below the proportion determined by chemical equilibrium (p/o = 1.18). In the case of MAPO-36 the selectivity to paraxylene is equal to or slightly higher than the equilibrium value, which is in agreement with the smaller channel opening (6.5 × 7.5 Å). The slight increase in the para/orthoxylene ratio with the Mg content in MAPO-36 is likely due to the larger size of the crystals when these contain more magnesium as showed previously (5). The values of the D/I ratio are below the unity and increase with the increase in the Mg fraction in the solid, which is due to the larger number of acid sites, as already discussed in the TPD results. Similar to the results found in other catalysts (8, 23, 24) the increase in acid site density enhances the probability that the reaction occurs by a bimolecular mechanism. The diffusional restrictions for this bimolecular reaction to take place inside the MAPO-36 channels would explain also the lower D/I ratio as compared to that of MAPO-5, despite the stronger acidity of the former.

The distribution of the trimethylbenzenes resulting from the disproportion reaction of *m*-xylene has been used to compare the apertures of the pores containing 12 tetrahedra (8). Figure 13 shows that the isomer with the smallest kinetic diameter (1,2,4-TMB) is formed at

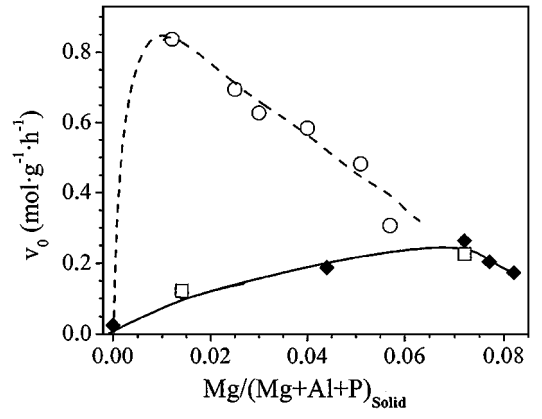

FIG. 11. Influence of magnesium content in MAPO-36 and MAPO-5 on the rate of *m*-xylene conversion. ○, MAPO-36. □, MAPO-5 calcined *in situ.* ◆, MAPO-5 *ex situ.*

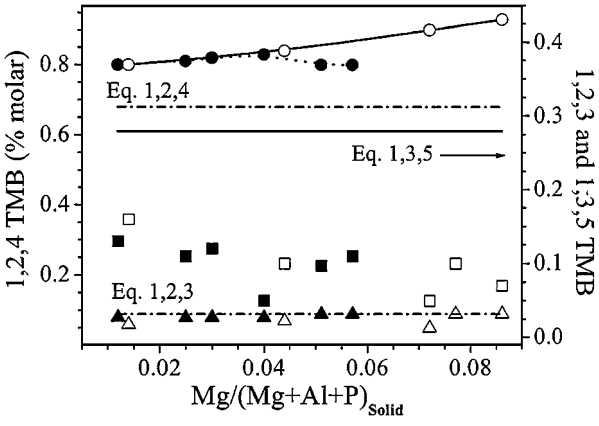

FIG. 13. Distribution of trimethylbenzene (TMB) as function of the Mg/(Mg + Al + P) ratio in MAPO-36 (solid) and MAPO-5 (open). ●,○, 1,2,4-TMB; ■,□, 1,3,5-TMB; ▲,△, 1,2,3-TMB.

proportions above equilibrium in detriment to the isomer with the larger diameter (1,3,5-TMB). Despite the fact that both materials possess large pore diameters, both structures are monodirectional, which makes diffusion of 1,3,5-TMB more difficult. Figure 13 also shows that the distribution of 1,2,4- and 1,3,5-TMB is a function of the Mg content, but the influence of the structure is not evident.

CONCLUSIONS

For similar Mg contents in the gel, a higher incorporation of Mg in the solid was observed for MAPO-5 compared to MAPO-36. This behavior was observed with aluminum isopropoxide as well as with pseudoboehmite, indicating that magnesium can be accommodated more easily in the AFI structure than in the ATS structure. In both MAPO-36 and MAPO-5 the concentration of Mg on the surface of the crystals is higher than that in the bulk and also increases with the increase of Mg in the solid.

Calcination of the samples removes part of framework Mg in both structures, remaining in the solid as extra-framework species. Mg extraction was more pronounced for samples with higher Mg contents, indicating a lower stability of the structure as the Mg content increases. Temperature-programmed desorption of ammonia from MAPO-36 samples indicated the presence of two types of acid sites, the major part being strong acid sites whose number increases with Mg content. In concordance with TPD results, IR measurements show that this material was able to retain pyridine at a desorption temperature of 673 K and has an acid strength superior to that of MAPO-5. However, a high fraction of acid sites disappear on calcining the samples in air. As a consequence, the activity of the MAPO-36 samples calcined *in situ* in the isomerization of *m*-xylene was higher than that of the samples calcined *ex situ* .

The activity of MAPO-36 in the *m*-xylene isomerization decreases as the magnesium content increases, regardless of the aluminum source used in the synthesis. However, the MAPO-36 samples obtained with aluminum isopropoxide are less active than those obtained with pseudoboehmite. The MAPO-5 activity did not vary significantly when the samples were calcined *in situ* or *ex situ*, suggesting that similar amounts of Mg are extracted from the AFI framework. As a consequence of the higher acid strength, the catalytic activity of MAPO-36 was much higher than that of MAPO-5 when the concentration of Mg in the crystals was low, although the difference reduces as the content of this element increases.

ACKNOWLEDGMENTS

M. da S. Machado acknowledges the CAPES for a Ph.D. grant. Financial support for this project by FAPESP (Project 96/4216-0) of Brazil and the Ministry of Education of Spain (Project MAT97-1207-CO3) is acknowledged.

REFERENCES

1. Meier, W. M., Olson, D. H., and Baerlocher, Ch., *Zeolites* **17**, 1 (1996).
2. Flanigen, E. M., *Stud. Surf. Sci. Catal.* **37**, 13 (1988).
3. Akolekar, D. B., *J. Catal.* **144**, 148 (1993).
4. Akolekar, D. B., *J. Catal.* **146**, 62 (1994).
5. Machado, M da S., Cardoso, D., Pérez-Pariente, J., and Sastre, E., *Chem. Mat.* **11**, 3238 (1999).
6. Concepción, P., López-Nieto, J. M., Mifsud, A., and Pérez-Pariente, J., *Zeolites* **16**, 56 (1996).
7. Prasad, S., Barich, H. D., and Haw, F. J., *Catal. Lett.* **39**, 141 (1996).
8. Martens, J. A., Pérez-Pariente, J., Sastre, E., Corma, A., and Jacobs, P. A., *Appl. Catal.* **45**, 85 (1988).
9. Parrillo, D. J., Pereira, C., Kokotailo, G. T., and Gorte, R. J., *J. Catal.* **138**, 377 (1992).
10. Wilson, S. T., and Flanigen, E. M., *in* "Zeolite Synthesis" (M. L. Ocelli and M. E. Robson, Eds.), Vol. 398, p. 329. ACS Symp. Series, Washington, DC, 1989.
11. Giotto, M. V., Machado, M da S., Pérez-Pariente, J., Rios, S. P. O., and Cardoso, D., *in* "Proceedings of the 12th International Zeolite Conference" (M. M. J. Treacy, B. K. Marcus, M. E. Bisher, and J. B. Higgins, Eds.), Vol. IV, p. 2481. MRS, Warrendale, PA, 1998.
12. Huang, M., Adnot, A., and Kaliaguine, S., *J. Catal.* **137**, 322 (1992).
13. Tossell, J. A., *J. Am. Chem. Soc.* **97**, 4840 (1975).
14. Haycock, D. E., Nicholls, C. J., Urch, D. S., Webber, M. J., and Wiech, G., *J. Chem. Soc. Dalton Trans.* 1785 (1978).
15. Machado, M da S., Pérez-Pariente, J., Cardoso, D., Sastre, E., Giotto, M. V., Blasco, T., and Mifsud, A., to be published.
16. Ono, Y., Nakashiro, K., Shin-ichi, N., and Morimura Y., *Zeolites* **13**, 561 (1993).
17. Montoya-Urbina M., Cardoso, D., Pérez-Pariente, J., Sastre, E., Blasco, T., and Fornés, V., *J. Catal.* **173**, 501 (1998).
18. Akolekar, D. B., *J. Catal*. **143**, 62 (1993).
19. Akolekar, D. B., *Zeolites* **14**, 53 (1994).
20. Nakashiro, K., and Ono, Y., *J. Chem. Soc. Faraday Trans.* **87**(19), 3309 (1991).
21. Lischke, G., Parlitz, B., Lohse, U., Schreier, E., and Fricke, R., *Appl. Catal.* **166**, 351 (1998).
22. Tromp, M., van Bokhoven, J. A., Oostenbrink, M. T. G., Bitter, J. H., de Jong, K. P., and Koningsberger, D. C., *J. Catal.* **190**, 209 (2000).
23. Morin, S., Gnep, N. S., and Guisnet, M., *J. Catal.* **159**, 296 (1996).
24. Lourenço, J. P., Ribeiro, M. F., Rocha, J., and Gabelica, Z., *Appl. Catal.* **148**, 167 (1996).